---

**Article:**
Wiessler, O. and Long, H. orcid.org/0000-0003-1673-1193 (2022) Design of single point incremental forming for a motorcycle headlight fairing manufacture. Key Engineering Materials, 926. pp. 822-833.

https://doi.org/10.4028/p-w67m8b

---

*Key Engineering Materials*
*ISSN: 1662-9795, Vol. 926, pp 822-833*
*doi:10.4028/p-w67m8b*

*Submitted: 2021-12-13*
*Revised: 2022-02-08*
*Accepted: 2022-02-08*
*Online: 2022-07-22*

# Design of Single Point Incremental Forming for a Motorcycle Headlight Fairing Manufacture

Oscar Wiessler[1,a] and Hui Long[1,b*]

[1]Department of Mechanical Engineering, the University of Sheffield, UK

[a]owiessler1@sheffield.ac.uk; [b*] h.long@sheffield.ac.uk (corresponding author)

**Keywords:** single point incremental forming, geometrical accuracy, finite element modelling, experimental validation.

**Abstract.** This paper presents a study of design of a motorcycle headlight fairing for single point incremental forming by employing a simplified design guideline in conjunction with a finite element simulation of the forming process. Comparison with the experimental formed motorcycle headlight fairing is performed based on a detailed analysis of geometric accuracy of the formed parts. The study may serve as a demonstration of capabilities of single point incremental forming with respect to dimensional accuracy when forming complex parts.

## 1 Introduction

Over the past few decades extensive research has been conducted into the development of new manufacturing and rapid prototyping techniques for sheet metal. In an era in which increasing value is placed on product differentiation and small batch manufacturing, new high flexibility manufacturing methods are required. Currently the most widely used sheet metal forming technique in industry is stamping, a process only economically viable for use in mass production where effective economies of scale can be achieved.

Single point incremental forming (SPIF) is based around a computer numerical controlled tool locally deforming a blank sheet of metal that is clamped around its perimeter. Developments in the SPIF process were first made by Iseki et al. [1, 2]. The process allows for high levels of process flexibility, whilst experimental work has shown that SPIF is able to achieve much higher strain states than traditional cold forming operations. Extensive research has been conducted into many different aspects of the process. Various toolpath approaches were developed to reduce sheet thinning, enhance formability and improve dimensional accuracy. These included multistage paths, feature based paths for specific regimes, varied up and down tool movement directions as well as in-process compensation for geometric error induced by spring back [3-7]. Process formability was another area that received research interest where maximum formable wall angle was frequently used as a metric to describe formability [4]. A variety of methods were used to ascertain this critical wall angle however its definition was somewhat unclear and was subject to inconsistency [5, 8]. The significant effect of process parameters such as tool diameter, vertical step, material and thickness also led to a lack of uniformity in the determination of the maximum forming angle for a specific process [9-12]. It was suggested that the lack of diffusion into industry of this highly flexible process was due to a lack of available knowledge outside of scientific and research communities and a relatively high level of geometric error of the process [13]. A detailed product characterisation was carried out by Allwood et al. [14] in conjunction with 41 companies producing sheet metal products. It highlighted that the most important improvement required in ISF was dimensional accuracy, where a working tolerance of 0.3mm could significantly increase the uptake of ISF in industry. It is the authors' belief that these problems can be addressed, to a certain extent, by the documented, analysed and disseminated forming of industry standard components.

Several experimental works developed industry relevant components using SPIF, focusing on the biomedical, aerospace and automotive industries. Ambrogio et al [15] conducted a detailed design and product analysis of a customised ankle support, utilising laser scanning methods to analyse the geometric accuracy of the component, demonstrating a working accuracy of 1mm. Several studies

investigated the manufacture of cranial implants, using SPIF. Duflou et al. [16] conducted a detailed study investigating the effects of compensating toolpaths on final component accuracy, achieving a minimum deviation of the finished cranio-facial implant of 0.834mm when utilising an error compensating toolpath regime. Lu et al. [17] also conducted detailed analysis of a titanium based cranial reconstruction, achieving a maximum error of 3mm between the designed and formed components. Notably this was the only study that investigated the thickness variation of the formed component. Vanhove et al. [18] also used compensating toolpaths to achieve a maximum geometric error of 0.3mm when forming a clavicle implant from titanium. Gupta et al [19] investigated the forming of an aerospace c-channel geometry with high wall angles, achieving a maximum geometric deviation of 1.5mm. Finally, the only work focusing on the automotive sector was performed by Duc-Toan et al. [20] who performed the coupled experimental and numerical forming of a scale vehicle tale gait. Despite investigating the level of geometric error between designed and simulation formed cross sections, this work failed to fully examine the geometric error in the experimentally formed cross section or draw comparison between the simulation and experimental results. Review of these examples clearly highlights a lack of relevant automotive component studies that conduct thorough geometric analysis of components formed from industry relevant materials.

Finite element (FE) analysis has been widely used to model incremental sheet forming. However, the long toolpaths and nonlinearities make a successful FE simulation relies heavily on reducing computational weight. Early research conducted by Ambrogio et al. [21] suggested that the use of the explicit FE method allowed for reasonably accurate prediction of formed component geometry and wall thickness variation. Further research has gone on to highlight the computational benefits of the explicit scheme when compared to the implicit method, assessing simulation accuracy and parameter optimisation. Notably Baranoglu et al. [22] made comparison between the implicit and explicit schemes through comparison with experimental forming of 3 geometries. Their work highlighted the computational advantages of the explicit scheme despite its inferior accuracy when compared to the implicit FE method. The careful optimisation of simulation parameters allowed for fast and accurate simulation of the forming process. Whilst their simulations all used the 4 node shell element, further research suggested that a linear brick element provided more accurate results [23]. Especially regarding thickness prediction where the brick elements were capable of capturing the through thickness shear that played an important stabilising role in SPIF deformation mechanics. Whilst mass scaling was commonly adopted to reduce the computational time of explicit simulations, Bambach [24] looked further at using adaptive remeshing and subcycling to further reduce computational times of explicit FE models. Despite large reductions in computational time this work failed to decouple this reduction from a decrease in simulation accuracy. Despite most of the aforementioned work being conducted on simple axisymmetric geometries several works have performed the coupled simulation and experimental forming of industrial standard parts. Nguyen et al. [25] formed a model of a human face as well as vehicle tailgate but failed to address the simulation accuracy with respect to the experimentally formed parts.

Some research highlighted the geometric constraints imposed by the SPIF process and in a few cases design guidelines were suggested for component design for SPIF manufacture. Adams and Jeswiet [4] focused on component wall angle as a key design parameter, a metric was established by using the novel thinning limit process defined by Hussain and Gao [8]. Alfonso et al. [26] furthered the work performed by Adams and Jeswiet [4], outlining a detailed set of feature specific design rules that not only allowed the designer to avoid component failure during manufacture, but also to reduced geometric errors, improved dimensional accuracy and surface finish. Despite a comprehensive design guide, Alfonso et al. [26] only produced one component to validate the reliability of their guidelines; further testing was required to confirm the validity of their design rules. Importantly none of the studies investigating design rules or performing experimental forming of industry standard components performed a detailed analysis of geometric accuracy of the formed components.

The objective of this study is to successfully design a motorcycle headlight fairing for SPIF manufacture using a simplified design guideline in conjunction with a FE simulation of the forming process. Comparison with experimental forming will be used to quantify the effectiveness of this design process and a detailed

analysis of the geometric errors of the parts will serve as a demonstration of capabilities of SPIF with respect to dimensional accuracy when forming complex parts.

## 2 Component Design Methodology

The automotive industry holds a significant share in the global sheet metal market and is an industry where the implementation of SPIF for rapid prototyping and low volume production could significantly improve product design cycles and reduce low volume production costs by as much as 90% [27]. This study focuses on designing an automotive component for SPIF manufacture in an attempt to further prove the process for industrial applicability. The design process will be based around the FE simulation of component manufacture. Although this faces several challenges it will set a platform from which industry may experiment with the process, without the need for SPIF specific equipment investment.

**Material Choice**. In this study, the aluminium alloy AA5251-H22 is chosen. The high level of ductility of this medium strength alloy makes it well suited for use with the SPIF process. AA5251-H22 is often used in industry, in vehicle panel applications [28]. Thus, its use provides continuity in the attempt to prove the industrial applicability of the SPIF process. In line with the key design-parameters suggested in literature the critical forming angle is determined through the experimental forming of a variable wall angle conical frustum. For AA5251-H22, the experimental data was recorded by Ai [29] which determined a thinning limit at 71.2 degrees. The thinning limit could be used as the critical forming angle as demonstrated by Hussain and Gao [8].

**Headlight Fairing Design.** Based on the design guidelines proposed by the aforementioned authors, a simplified design guide is produced to allow the motorcycle headlight fairing to be designed for SPIF manufacture. This is presented in Table 1. Following the detailed design guide and based on industry standards, two designs of a motorcycle headlight fairing, Design Model-1 and Design Model-2, are developed, as shown in Fig. 1. The first design is intended to test the process limits, as such it includes a high maximum wall angle of 70 degrees, close to the experimentally determined maximum wall angle for the chosen process parameters. Importantly the design also exhibits limited asymmetry and walls of varying curvature. The second design follows a more conservative approach that falls well within process limits with the aim of optimising the quality of the finished component. This includes a lower maximum wall angle of 55 degrees, increased levels of asymmetry and constant wall angle in the area of highest wall angle.

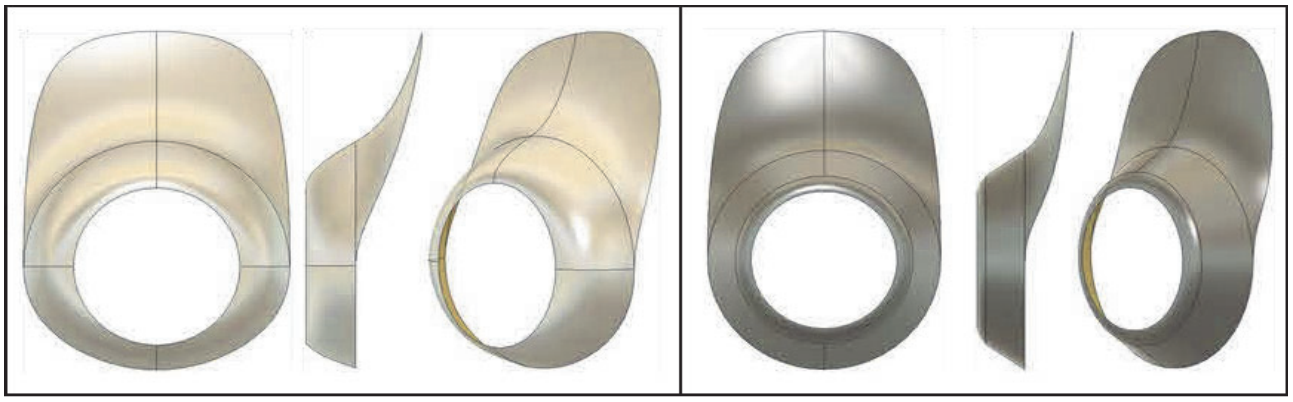

**Fig. 1** Headlight fairing designs, maximum limit Model-1(left) and conservative design Model-2 (right)

**Table 1** SPIF design guidelines developed from literature

| | **Fundamental Rules to Avoid Failure** | | | | **Guildelines to Improve Dimensional and Geometric Accuracy** | | | | | |
|---|---|---|---|---|---|---|---|---|---|---|
| *Rule* | Critical wall angle | Convex to concave | Internal corner radius | Working area | Changes in curvature | Large shallow sloped regions | Large flat regions | Small corner radius at blank top | Large radius between walls and base | Small detailed features |
| *Design Action* | Maximum wall angle below critical value | Single concave features only | Minimum internal radius equal to or greater than tool | Maximum dimension within woking area | Minimise where possible | Minimise where possible | Minimise where possible | Use small corner radius iof possible | Minimise where possible | Ensure critical dimension is greater that 2x sheet thickness |

## 3 Finite Element Modelling and Experimental Validation

**Finite Element Modelling.** The FE package Abaqus is used to conduct an explicit FE analysis of the SPIF of the motorcycle headlight fairing. The explicit method solves the FE problem without iteration and is far more computationally efficient than an implicit equivalent [30]. The explicit scheme allows the use of artificial mass scaling where fixed mass scaling with a minimum stable time increment of 5e-05 is employed for all simulations. The general-purpose linear brick element with reduced integration, C3D8R, is used based on the successful work of Ai et al. [31], where five through thickness elements with a global size of 0.5mm produced mesh independent results. Due to the extremely large number of increments used, to simulate the long toolpaths of SPIF, it is vital to use a double precision regime in Abaqus to reduce the cumulative rounding error that can lead to poor toolpath definition.

**Material Flow Stress.** Due to the high strains experienced in the SPIF process the true plastic stress-strain curve of AA5251 H22, obtained from the uniaxial tensile test, does not adequately describe the material deformation. The Voce hardening law is employed to approximate the extension of the flow stress curve to higher strain values.

**Toolpath.** The toolpath generation for FE simulation of SPIF involves several steps, where the most accurate toolpath definition is established using a commercial CAM package. A helical toolpath regime is employed to minimise surface scarring and improve thinning uniformity. Key toolpath parameters used are a tool radius of 5mm, feed rate of 2000mm/min and a scallop height of 0.05mm. For use with the FE simulation, in Abaqus, the G-code file must be converted into a Cartesian coordinate vs time dataset and each linear tool movement time increment is calculated.

**FE Model Verification.** To verify the effect of mass scaling on the simulation accuracy it is important to ensure that the artificial mass increase does not cause unwanted effects and that inertia does not become dominant. This is established by monitoring the energy history of the simulation.

**Experimental Setup.** For the experimental forming setup, a 3-axis precision milling centre is used in conjunction with a SPIF specific blank clamping fixture. The key forming parameters used are following best practice where an oil lubricant and fixed rotation tool is used. The feed rate used is 1500mm/s, this is lower than that used in the simulated forming process due to machine limitations, however several works have highlighted the limited effect of tool feed rate on the forming process.

**Measurement of Geometry Profiles.** The assessment of the formed geometries is performed using a class leading MCAs+ 3.5m scanner arm in conjunction with a Nikon H120 laser scanner, providing a repeatability of +/- 0.007mm. The laser scanner generates a point cloud that allows for conversion into a suitable format for digital comparison.

## 4 Results and Discussion

### 4.1 Design Model-1: Maximum Limit Design Geometry

**Stress.** von Mises stress is used in the FE analysis of the stress state experienced during deformation. A maximum von Mises stress value of 224MPa is shown during the forming process, Fig.2. This is equal to the maximum stress value of the Voce law extended flow stress curve for AA5251 H22. As the forming process is characterised by large plastic deformation, high strains are experienced which fall outside of those experienced in the uniaxial tensile test and deformation acts in the extended region of the flow stress curve. The stress output reaches its maximum value early in the simulation, as plastic strain becomes large. As such, von Mises stress does not provide a useful insight into the deformation of the geometry. Although the Voce law provides a good fit to the experimental data generated by the tensile test, this does not fully account for the complex deformation modes experienced in SPIF, specifically cyclic bending under tension with through thickness shear [32]. More sophisticated constitutive models are required in this respect to further improve simulation accuracy, especially if formed component testing is required.

**Strain.** Equivalent plastic strain, PEEQ in Abaqus, is a useful measure of the total strain experienced. The equivalent plastic strain distribution, Fig. 2, shows that a high maximum value of 2.859 is experienced in the steepest walls of the deformed part. This is possible due to the stabilising mechanisms in the SPIF process, where strains can reach values up to 300% [5]. The lack of symmetry in the equivalent plastic strain distribution is due to the clockwise direction of tool movement and non-axisymmetric design. A bidirectional toolpath regime could provide a more evenly distributed strain state.

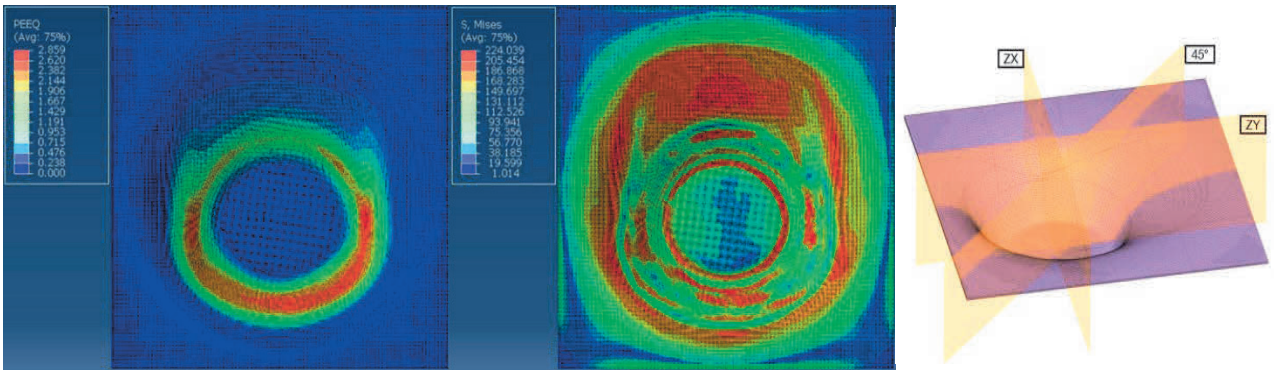


**Fig. 2** Design Model-1: distributions of equivalent plastic strain (left), von Mises stress (centre), definitions of ZY and ZX cross sections (right)

**Experimental Validation.** Validation with experimental data is performed to definitively quantify the level of geometric accuracy of the FE model. This is especially important as artificial mass scaling is applied to reduce the computational time of the simulation. Due to the complexity involved with comparing the experimentally formed and simulated geometry, two cross sections (0,Y,Z) and (X,0,Z), as shown in Fig. 2, are chosen as critical planes in which the geometry is assessed to evaluate the FE model. As shown in Fig. 3, there is good agreement between the simulation formed geometry and the experimentally formed one, for both the overall geometry and the wall thickness variation. There is a general deviation of less than +/- 0.2mm. Near the edge of the component, significant spring back and deformation are experienced when the blank is removed from the clamping. Because the blank removal from the clamp is not modelled in FE, it will cause the higher level of error seen in Fig. 3. In both the simulated and experimental geometry, the greatest thinning is experienced in the area of highest wall angle, in region A, as shown in Fig. 3. Comparison indicates that FE modelling can provide a reasonable prediction of the thinning behaviour underestimating the thinning by 3.9%.

**Thickness distribution.** The thickness distribution of the entire part is analysed. The cross section experiencing the most severe thinning is investigated. A minimum wall thickness of 0.291mm is experienced in section A of Fig. 3. This severe level of thinning is characteristic of the SPIF process at high wall angles where the thickness variation highlighted in Table 2, is due to the varying wall

angle and does not suggest necking behaviour. Previous research has shown that AA5051 does not experience necking before failure in the SPIF process [33]. From a design perspective, the non-uniform wall thickness in conjunction with high levels of thinning might not be desirable depending on the product's use case. Non-uniform thinning where variable wall angle components are used is something that must be considered in the SPIF design process. Comparison with the analytical value predicted by the sine rule highlights that the sine rule is not capable of accurately predicting wall thicknesses for complex components formed using SPIF, in agreement with literature.

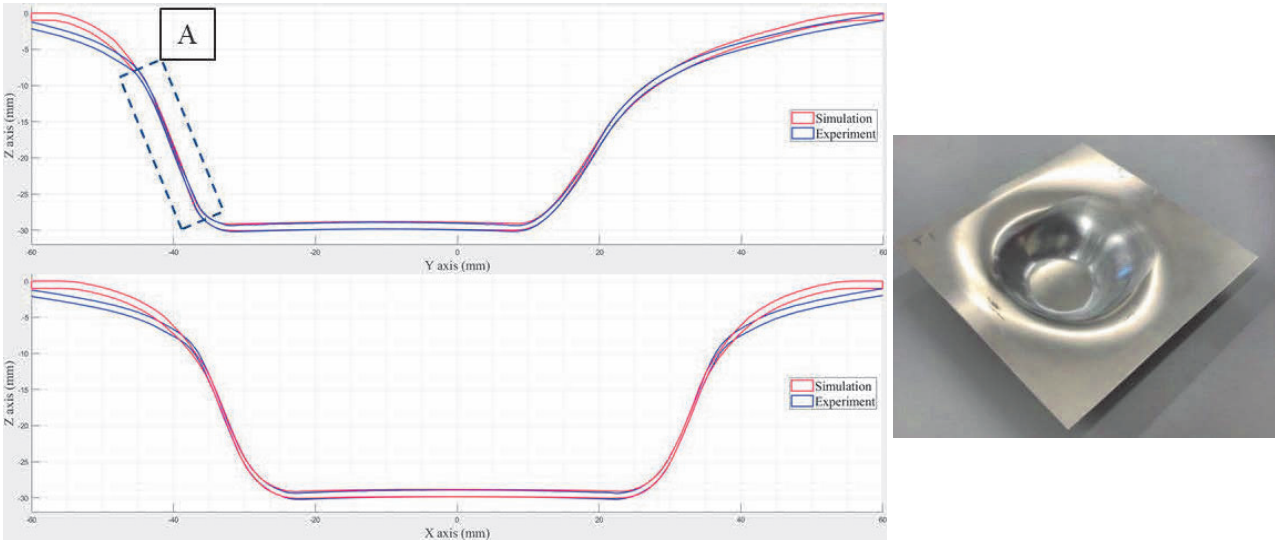


**Fig. 3** Design Model-1: Comparison between simulated and experimentally formed geometries in ZY and ZX cross sections (left) and the formed part picture (right)

**Table 2** Design Model-1: wall thickness variation in the critical wall section

| | Minimum Wall Thickness (mm) | Error with Experiment (%) | Max Thickness in Critical Wall (mm) | Error with Experiment (%) |
|---|---|---|---|---|
| *Simulation* | 0.291 | 3.9 | 0.443 | 1.14 |
| *Sine Rule* | 0.34 | 21.4 | 0.57 | 30 |
| *Experimental* | 0.28 | - | 0.438 | - |

**Table 3** Design Model-1: maximum geometric error in the formed geometry in key areas in Fig. 4

| Cross Section | Section | A | B | C | D | E |
|---|---|---|---|---|---|---|
| ZY | Maximum Normal Error (mm) | 3.98 | 0.82 | 0.58 | 0.15 | 1.64 |
| ZX | Maximum Normal Error (mm) | 4.68 | 0.47 | 0.58 | - | - |

**Geometry Analysis.** Comparison is made between the experimentally formed geometry and the designed inner surface geometry. Fig. 4 highlights the comparison between the designed surface and the formed part. The error in all key locations is identified and quantified in Table 3. It is summarised that the maximum level of error occurs at the top of the workpiece due to bending of the blank, highlighted in sections A and E, Fig. 4. All other significant geometric errors are below 1mm in magnitude and can be accounted for by spring back during the forming process, a geometric error that has been identified in numerous studies. Importantly, the relatively high error experienced in section B of 0.82mm might be due to the excessive thinning in this region. In the case of this design, it must be considered that after trimming from the blank, to produce the finish part shown in Fig. 1, the largest identified errors caused by bending of the blank and spring back will be removed, leaving the final part with a maximum geometric error of 0.82mm, highlighted in Table 2. This is in line with the level of accuracy experienced in literature. However, further spring back and distortion during trimming could further affect the final part accuracy, this requires further investigation. The surface deviation plot in

Fig.4, obtained from the laser scan, is an average point cloud alignment and represents the minimised average deviation, in this case 0.9mm.

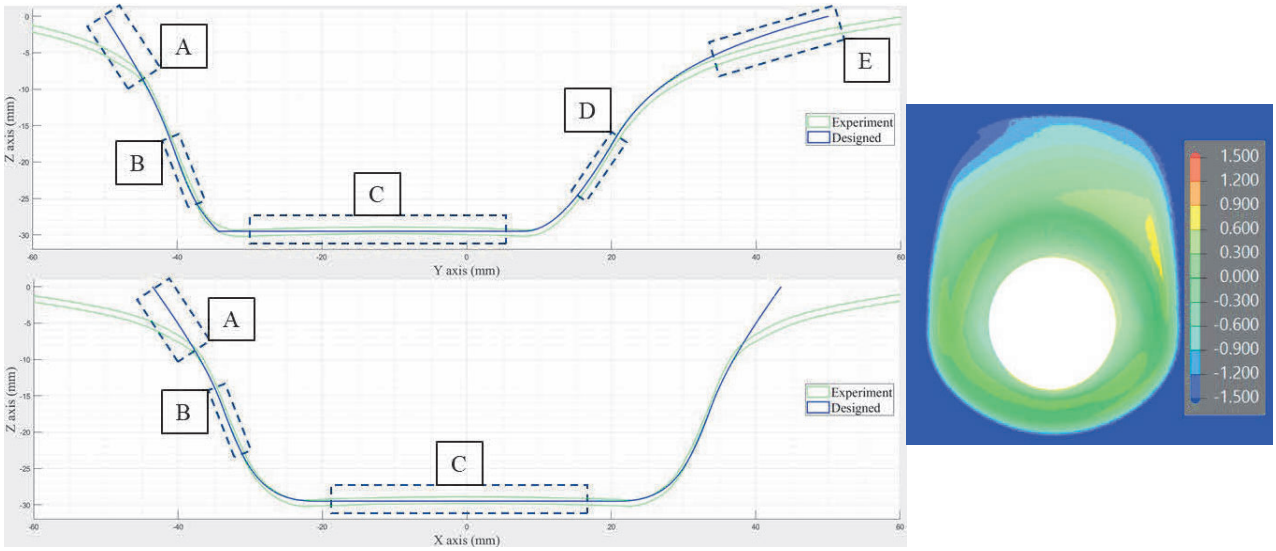


**Fig. 4** Design Model-1: comparison between formed and designed geometry in ZY and ZX cross sections (left) and 3D laser scan deviation plot in mm (right)

### 4.2 Design Model-2: Conservative Design Geometry.

As mentioned in Section 2, the second design Model-2 is based on a more conservative set of design principles to produce a 'safe' part that addresses some of the issues experienced with high levels of non-uniform thinning experienced in Design Model-1.

**Stress and strain.** As with the previous geometry, the maximum stress values give little insight into the deformation process other than to highlight the areas in which the strain has become high during deformation. As shown in Fig.5, there is a significant reduction in the equivalent plastic strain value as 2.208, when compared to the Design Model-1. This is due to the lower draw depth and reduced wall angle. It can be noted that the uniformity of the equivalent plastic strain distribution has greatly improved due to the increased levels of asymmetry of the conservative design.

**Experimental Validation.** Comparison between the simulation and experimentally formed geometries in the critical cross sections, Fig. 6, again confirms the ability of the simulation to deliver a high level of geometric accuracy in its prediction of the SPIF formed geometry. In the case of Design Model-2, the maximum deviation is less than +/- 0.1mm, excluding the areas near the edges of the blank in which the experimentally formed part has experienced spring back and distortion. The highlighted section A also exhibits a higher error of 0.59mm, it is suggested that this is also not an error in the simulated geometry but an effect of spring back upon removal from the clamping.

**Thickness Distribution.** The area in which the greatest thinning is experienced is identified and analysed, this is highlighted in Fig. 6, section B. The reduced level of thinning and increased uniformity, shown in Table 4, produces a component with increased mechanical strength and stiffness making it far more suitable for use in a practical application. This is obtained by reducing the designed wall angle to one well below the critical wall angle, as well as using constant wall angles in the critical walls of the component.

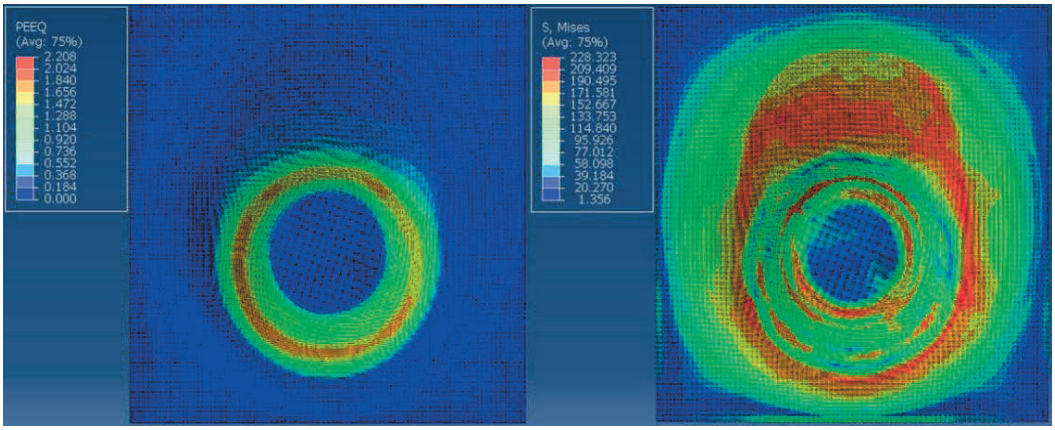


**Fig. 5** Design Model-2: distribution of equivalent plastic strain (left) and von Mises stress (right)

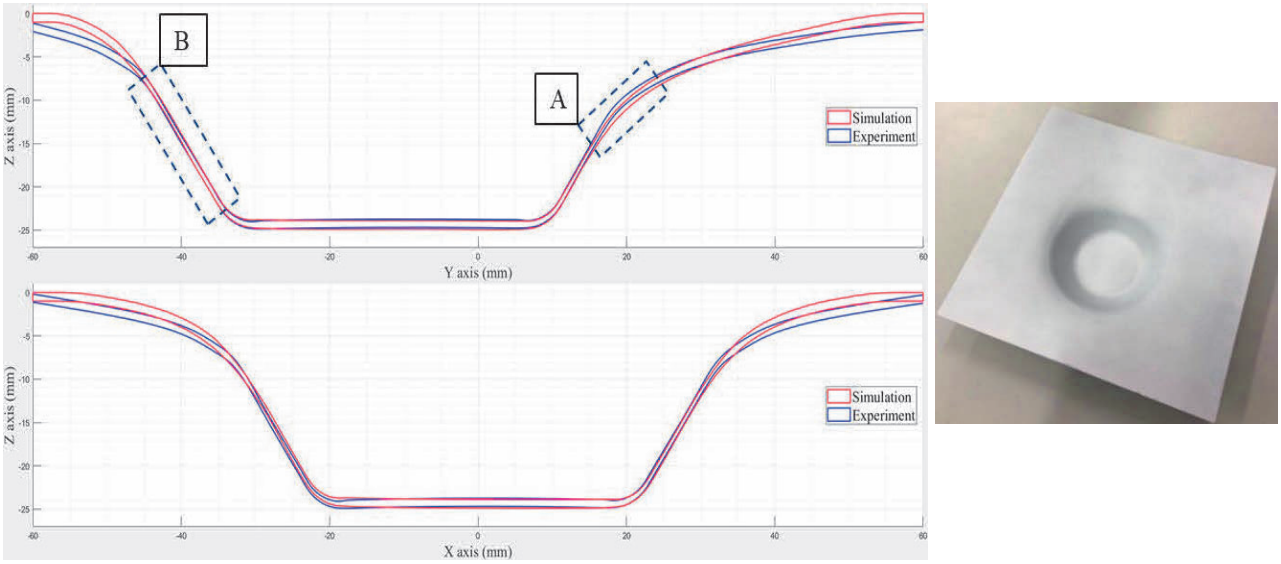


**Fig. 6** Design Model-2: Comparison between simulated and experimentally formed geometries in ZY and ZX cross sections (left) and the formed part picture (right)

**Table 4** Design Model-2: wall thickness variation in the critical wall section

| | Minimum Wall Thickness (mm) | Error with Experiment (%) | Maximum Thickness in Critical Wall (mm) | Error with Experiment (%) |
|---|---|---|---|---|
| *Simulation* | 0.488 | 1.6 | 0.54 | 8 |
| *Sine Rule* | 0.57 | 18.8 | 0.57 | 14 |
| *Experimental* | 0.48 | - | 0.5 | - |

**Table 5** Design Model-2: maximum geometric error in the formed geometry in key areas identified in Fig. 7

| Cross Section | Section | A | B | C | D | E |
|---|---|---|---|---|---|---|
| ZY | Maximum Normal Error (mm) | 3.51 | 0.16 | 0.35 | 0.35 | 2.04 |
| ZX | Maximum Normal Error (mm) | 2.63 | 0.28 | 0.35 | - | - |

**Geometry Analysis.** Comparison between the simulation formed geometry and the designed surface geometry allows for the level of error to be quantified in the two critical cross sections identified previously. The maximum normal errors are presented in Table 5. This highlights that the conservative design can achieve a higher level of geometric accuracy in all areas of the component. With a maximum error in the trimmed component area of 2.04mm due to bending at the top of the blank, whilst only 0.35mm in the high deformation regions that are not subject to this phenomenon. It is suggested that this overall improvement in geometric accuracy with respect to Design Model-1 is due to the reduced thinning and increased wall section uniformity, highlighting that this is an important consideration when designing parts for SPIF. It is also clear that flat sloped regions of lower deformation are prone to large distortion upon removal from the clamping, highlighted in section E of Fig. 7 and quantified in Table 5.

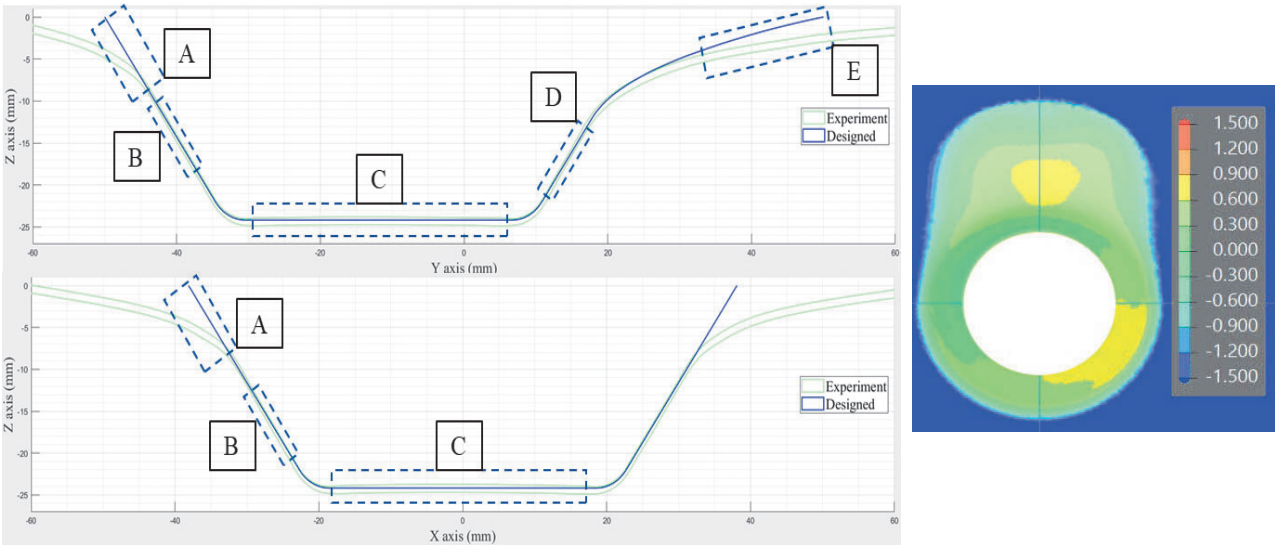


**Fig. 7** Design Model-2: comparison between formed and designed geometry in ZY and ZX cross sections (left) and 3D laser scan deviation plot in mm (right)

## 4.3 Discussion

The aim of this study is to determine if through using a combination of simplified design rules and FE modelling of the SPIF process, industry standard automotive parts can be designed and developed for successful manufacture. Comparison with two experimentally formed geometries has validated the FE modelling method and has demonstrated that it can accurately predict the geometry and importantly through thickness variation of SPIF formed parts. The FE model does not currently have the ability to capture the effects of spring back during the removal of the blank from the clamping. It is also important to note that although the FE model captures the geometry accurately it will likely not capture the mechanical properties of the final component due to limitations of the simplified FE model and the complex deformation that takes place during SPIF. This would become a problem when conducting formed part testing in conjunction with FE manufacture process simulation. An obvious downside to the FE simulation of SPIF is the long computational times even for relatively simple models when compared to the comparatively short forming times in the experimental approach. However, it is far easier and less time consuming to analyse the geometry of the finished component from FE simulated results than it is experimentally, requiring complex procedures and large equipment investment for geometric profile scanning.

A major limitation of the FE simulation approach is when design and forming parameters are such that the component is likely to experience failure during forming. Without the additional material damage models, the FE model is not capable of predicting failure in the SPIF process. In the case of this study and any work that carefully applies the aforementioned design rules to the component design, this is not a problem as failure is unlikely to occur in the formed part and the FE simulation can accurately predict the formed component geometry. The failure mechanisms at play in SPIF have been

summarised by Ai et al [33] and it has been shown that, in many cases, failure occurs without necking. One of the reasons why forming limit diagrams, widely employed with traditional sheet forming processes, cannot be used with the SPIF process. However, in many cases fracture forming diagrams can accurately predict SPIF failure and could be used in conjunction with the FE model developed in this study, serving as an improvement to this design process.

This study has highlighted that maximising the use of constant component wall angles can be a good strategy to improve the wall thickness uniformity. In conjunction with using lower wall angles, where possible, the geometric accuracy of the component can be significantly improved. It is suggested that this is due to an improvement in mechanical stiffness of the component walls, minimising spring back during forming. The relationship between the maximum designed and critical wall angles and its effect on geometric accuracy should be further investigated. Although the effects of variation in wall angle on failure have been investigated, their relationship to component geometric accuracy should be further interrogated.

Whilst this study has proved that SPIF can provide a low level of geometric error throughout the majority of the component, the elastic spring back near the clamped edges of the part must be addressed. Further research is required to develop methods to minimise the residual stresses in the formed component that likely cause this phenomenon.

## 5 Conclusion

This study has demonstrated the ability of a FE model to accurately capture the geometry of a SPIF formed motorcycle headlight fairing, to an acceptable level of accuracy. It has also shown that in conjunction with simple design guidelines the FE model can be used to develop industry standard automotive componentry where SPIF is capable of forming the components to a good level of accuracy. New design guides have been suggested to help improve component geometric accuracy and thickness uniformity however further investigation is required to evaluate these. It is suggested that the relationship between the maximum designed and critical wall angles and its effect on geometric accuracy should be further investigated.

## Acknowledgements

The authors would like to acknowledge the funding support received from the UK EPSRC through project grant EP/T005254/1. The authors would also like to thank Dr Wenxuan Peng and Mr. Jamie Booth of the Department of Mechanical Engineering for their assistance in the experimental forming of the motorcycle headlight fairing. Finally, the authors would like to thank Laser Scanning Limited and Mr. Johnathan Rigby for their crucially important help in the inspection of the formed motorcycle headlight fairing.

## References

[1] H. Iseki, K. Kato, and S. Sakamoto, Forming limit of flexible and incremental sheet metal bulging with a spherical roller, *Proc. 4th ICTP*, pp. 1635–1640, 1993.

[2] E. Hagan and J. Jeswiet, A review of conventional and modern single-point sheet metal forming methods, *Proc. Inst. Mech. Eng. Part B J. Eng. Manuf.*, 217(2) (2003) 213–225, doi: 10.1243/095440503321148858.

[3] F. Micari, G. Ambrogio, and L. Filice, Shape and dimensional accuracy in Single Point Incremental Forming: State of the art and future trends, *J. Mater. Process. Technol.*, 191(1–3) (2007) 390–395, doi: 10.1016/j.jmatprotec.2007.03.066.

[4] D. Adams and J. Jeswiet, Design rules and applications of single-point incremental forming, *Proc. Inst. Mech. Eng. Part B J. Eng. Manuf.*, 229(5) (2015) 754–760, doi: 10.1177/0954405414531426.

[5] J. Jeswiet and D. Young, Forming limit diagrams for single-point incremental forming of aluminium sheet, *Proc. Inst. Mech. Eng. Part B J. Eng. Manuf.*, 219(4) (2005) 359–364, doi: 10.1243/095440505X32210.

[6] M. Skjoedt, N. Bay, B. Endelt, and G. Ingarao, Multi Stage Strategies for Single Point Incremental Forming of a Cup, *Int. J. Mater. Form.*, 1(2008) 185–188, doi: 10.1007/s12289-008-0156-3.

[7] M. Skjoedt, M. B. Silva, P. A. F. Martins, and N. Bay, Strategies and limits in multi-stage single-point incremental forming, *J. Strain Anal. Eng. Des.*, 45(1) (2010) 33–44, doi: 10.1243/03093247JSA574.

[8] G. Hussain and L. Gao, A novel method to test the thinning limits of sheet metals in negative incremental forming, *Int. J. Mach. Tools Manuf.*, 47(3–4) (2007) 419–435, doi: 10.1016/j.ijmachtools.2006.06.015.

[9] G. Hussain, N. U. Dar, L. Gao, and M. H. Chen, A comparative study on the forming limits of an aluminum sheet-metal in negative incremental forming, *J. Mater. Process. Technol.*, 187–188 (2007) 94–98, doi: 10.1016/j.jmatprotec.2006.11.112.

[10] M. Ham and J. Jeswiet, Single point incremental forming and the forming criteria for AA3003, *CIRP Ann. - Manuf. Technol.*, 55 (1) (2006), 241–244, doi: 10.1016/S0007-8506(07)60407-7.

[11] L. Fratini, G. Ambrogio, R. Di Lorenzo, L. Filice, and F. Micari, Influence of mechanical properties of the sheet material on formability in single point incremental forming applied to manufacturing of biocompatible polymer prostheses forming, CIRP Ann. - Manuf. Technol., 53 (1) (2004) 207–210.

[12] G. Hussain, H. R. Khan, L. Gao, and N. Hayat, Guidelines for tool-size selection for single-point incremental forming of an aerospace alloy, *Mater. Manuf. Process.*, 28(3) (2013) 324–329, doi: 10.1080/10426914.2012.700151.

[13] J. Jeswiet, F. Micari, G. Hirt, A. Bramley, J. Duflou, and J. Allwood, Asymmetric single point incremental forming of sheet metal, *CIRP Ann. - Manuf. Technol.*, 54(2) (2005) 88–114, doi: 10.1016/s0007-8506(07)60021-3.

[14] J. M. Allwood, G. P. F. King, and J. Duflou, A structured search for applications of the incremental sheet-forming process by product segmentation, in *Proceedings of the Institution of Mechanical Engineers, Part B: Journal of Engineering Manufacture*, Feb. 2005, 219(2) 239–244, doi: 10.1243/095440505X8145.

[15] G. Ambrogio, L. De Napoli, L. Filice, F. Gagliardi, and M. Muzzupappa, Application of Incremental Forming process for high customised medical product manufacturing, *J. Mater. Process. Technol.*, 162–163 (2005) 156–162, doi: 10.1016/j.jmatprotec.2005.02.148.

[16] J. R. Duflou, A. K. Behera, H. Vanhove, and L. S. Bertol, Manufacture of accurate titanium cranio-facial implants with high forming angle using single point incremental forming, in *Key Engineering Materials*, 549 (2013) 223–230, doi: 10.4028/www.scientific.net/KEM.549.223.

[17] B. Lu, H. Ou, S. Q. Shi, H. Long, and J. Chen, Titanium based cranial reconstruction using incremental sheet forming, *Int. J. Mater. Form.*, 9(3) (2016) 361–370, doi: 10.1007/s12289-014-1205-8.

[18] H. Vanhove, Y. Carette, S. Vancleef, and J. R. Duflou, Production of thin Shell Clavicle Implants through Single Point Incremental Forming, in *Procedia Engineering*, 183 (2017) 174–179, doi: 10.1016/j.proeng.2017.04.058.

[19] P. Gupta, A. Szekeres, and J. Jeswiet, Design and development of an aerospace component with single-point incremental forming, *Int. J. Adv. Manuf. Technol.*, 103(9–12) (2019) 3683–3702, doi: 10.1007/s00170-019-03622-4.

[20] N. Duc-Toan, Y. Seung-Han, J. Dong-Won, C. Tae-Hoon, and K. Young-Suk, Incremental sheet metal forming: Numerical simulation and rapid prototyping process to make an automobile white-body, *Steel Res. Int.*, 82(7) (2011) 795–805, doi: 10.1002/srin.201000284.

[21] E. Oñate, D. R. J. Owen, G. Ambrogio, L. Filice, F. Gagliardi, and F. Micari, THREE-DIMENSIONAL FE SIMULATION OF SINGLE POINT INCREMENTAL FORMING: EXPERIMENTAL EVIDENCES AND PROCESS DESIGN IMPROVING. [Online]. Available: www.unipa.it.

[22] B. Baranoğlu *et al.*, Simulation for Incremental Sheet Forming Process: a Comparison of Implicit and Explicit Finite Element Analysis with Experimental Data, 2013. [Online]. Available: https://www.researchgate.net/publication/279911242.

[23] P. Gupta and J. Jeswiet, Parameters for the FEA simulations of single point incremental forming, *Prod. Manuf. Res.*, 7(1) (2019) 161–177, doi: 10.1080/21693277.2019.1608330.

[24] M. Bambach, Fast simulation of incremental sheet metal forming by adaptive remeshing and subcycling, *Int. J. Mater. Form.*, 9(3) (2016) 353–360, doi: 10.1007/s12289-014-1204-9.

[25] D. T. Nguyen, J. G. Park, H. J. Lee, and Y. S. Kim, Finite element method study of incremental sheet forming for complex shape and its improvement, *Proc. Inst. Mech. Eng. Part B J. Eng. Manuf.*, 224(6) (2010) 913–924, doi: 10.1243/09544054JEM1825.

[26] D. Afonso, R. Alves de Sousa, and R. Torcato, Integration of design rules and process modelling within SPIF technology-a review on the industrial dissemination of single point incremental forming, *Int. J. Adv. Manuf. Technol.*, 94(9–12) (2018),4387–4399, doi: 10.1007/s00170-017-1130-3.

[27] Grand View Research, Sheet Metal Market Size, Share & Trends Analysis Report By Material (Steel, Aluminum), By End-Use (Automotive & Transportation, Building & Construction), By Region, And Segment Forecasts, 2019 - 2025, 2019. https://www.grandviewresearch.com/industry-analysis/sheet-metal-market.

[28] Aalco, 5754 - H22 Sheet and Plate, *Website*, pp. 2–3, 2015, [Online]. Available: http://www.aalco.co.uk/datasheets/Aluminium-Alloy-5754-H22-Sheet-and-Plate_153.ashx.

[29] S. Ai, ANALYSIS OF MATERIAL DEFORMATION AND FRACTURE MECHANISM IN INCREMENTAL SHEET FORMING BY SIMPLIFIED TESTING METHODS, PhD Thesis, The University of Sheffield, 2020.

[30] Abaqus_MIT, Explicit dynamic analysis, *abaqus-docs*, 2017. https://abaqus-docs.mit.edu/2017/English/SIMACAEANLRefMap/simaanl-c-expdynamic.htm.

[31] S. Ai, R. Dai, and H. Long, Investigating formability enhancement in double side incremental forming by developing a new test method of tension under cyclic bending and compression, *J. Mater. Process. Technol.*, 275, no. January 2019, p. 116349, 2020, doi: 10.1016/j.jmatprotec.2019.116349.

[32] W. C. Emmens and A. H. van den Boogaard, An overview of stabilizing deformation mechanisms in incremental sheet forming, *J. Mater. Process. Technol.*, 209(8) (2009) 3688–3695, doi: 10.1016/j.jmatprotec.2008.10.003.

[33] S. Ai, B. Lu, J. Chen, H. Long, and H. Ou, Evaluation of deformation stability and fracture mechanism in incremental sheet forming, *International Journal of Mechanical Sciences*, 125, no. December 2016, pp. 174–184, 2017, doi: 10.1016/j.ijmecsci.2017.03.012.